Applied Surface Science 466 (2019) 92–98

Contents lists available at ScienceDirect

Applied Surface Science

journal homepage: www.elsevier.com/locate/apsusc

Full Length Article

Interface engineering of Co_3O_4 loaded $CaFe_2O_4/Fe_2O_3$ heterojunction for photoelectrochemical water oxidation

Jiajia Cai[a], Song Li[b,*], Gaowu Qin[b]

[a] School of Energy and Environment, Anhui University of Technology, Maanshan, Anhui 243002, China
[b] Key Laboratory for Anisotropy and Texture of Materials (MoE), School of Materials Science and Engineering, Northeastern University, Shenyang 110819, China

ARTICLE INFO

Keywords:
$CaFe_2O_4/\alpha\text{-}Fe_2O_3$
Co_3O_4
Charge separation
Surface states
Photoelectrochemistry

ABSTRACT

Considerable efforts have been made to develop hematite as a promising material for photoelectrochemical (PEC) water splitting. However, the fast recombination of carriers in the bulk and on the surface greatly constrains the solar-to-chemical fuel conversion efficiency. Herein, a precise method was utilized to alleviate the recombination by constructing p-n junction of $CaFe_2O_4/\alpha\text{-}Fe_2O_3$ and further modifying with Co_3O_4. The structural information and chemical composition of the ternary compound were systematically characterized. The photocurrent density at 1.23 V vs RHE (reversible hydrogen electrode) of the photoanode increased by five times compared to the bare $\alpha\text{-}Fe_2O_3$, and the onset potential also shifted negatively to 0.6 V vs RHE. The formation of p-n junction and surface Co_3O_4 modification were proven to enhance the charge separation in the bulk and on the surface, respectively. Also the Co_3O_4 played a bifunctional role of passivating the surface states and accelerating the water oxidation kinetics.

1. Introduction

Photoelectrochemical (PEC) oxidation of water to O_2 over semiconducting photoanode is attracting intensive interests because the reaction sustainably provides cost-effective electrons for turning CO_2 and water into chemical fuels [1–3] or protecting steels from corrosion [4]. Among numbers of candidate semiconductors, hematite ($\alpha\text{-}Fe_2O_3$) receives the most intensive studies as both a promising photoanode material and a model platform to study the oxygen evolution reaction (OER) due to its favorable band gap, low cost, and chemical stability [3,5–7]. Though considerable works with remarkable achievements have been carried out, the reported PEC performance of $\alpha\text{-}Fe_2O_3$ remains far below the theoretical limit anticipated based on its light absorption properties. The unsatisfactory performance is now recognized as resulting from several limiting factors, including the mismatch between light absorption depth and hole collection length [3], the fast recombination of photocarriers both in the bulk and on the surface [6,8], and the sluggish water oxidation kinetics [9].

To breakthrough the limiting restrains, corresponding strategies have been proposed and practiced, including nanostructuring [10–12], chemical doping [13–15], surface modification [16–19], orientation control [20,21], heterojunction construction [22–24], and the combinations of the above [25–29]. By synthesizing low-dimensional nanostructured hematite of various morphologies, the distance that photoholes should travel to be collected could be minimized without sacrificing the light absorption [10]. Due to the extremely short diffusion length of minorities in hematite (2–4 nm), the recombination still occurs in the bulk region not far from the surface, especially when the electrode is slightly polarized. To address this constraint, coupling hematite with a suitable p-type semiconductor to form the p-n junction could be very promising. For example, a notable cathodic shift of the photocurrent onset potential was produced by a conformal p-type layer of Mg-doped $\alpha\text{-}Fe_2O_3$ [30]. But the preparation process needs to be precisely regulated by atomic layer deposition (ALD) method. As a typical intrinsic p-type semiconductor with visible light response [31], $CaFe_2O_4$ has been used to form p-n heterojunctions to improve the charge separation efficiency of series of materials [32–35]. Despite the photocurrent densities were increased by forming $CaFe_2O_4/\alpha\text{-}Fe_2O_3$ heterojunction [24], the structural information and the mechanism need to be further clarified. Similar role has been verified over hydrothermally synthesized $CaFe_2O_4/\alpha\text{-}Fe_2O_3$, though the photocurrent density was as low as $\sim 1\ \mu A/cm^2$ [36]. It is necessary to engineer the heterojunction interface by adjusting the distributions of $CaFe_2O_4$ over $\alpha\text{-}Fe_2O_3$. In addition, enhanced OER performance has been reported by surface decoration with Co_3O_4. However, the mechanism of Co_3O_4 remains controversial. Some researchers ascribed the positive effects of cobalt oxide to the suppression of surface recombination by passivating the surface states [37–39], while others attributed to the catalytic

---

[*] Corresponding author.
E-mail address: lis@atm.neu.edu.cn (S. Li).

https://doi.org/10.1016/j.apsusc.2018.10.022
Received 19 March 2018; Received in revised form 29 September 2018; Accepted 3 October 2018

effects [10,40,41]. Therefore, more studies are needed to elucidate the role of Co_3O_4.

In this work, the three-dimensional (3D) $CaFe_2O_4/\alpha\text{-}Fe_2O_3$ p-n heterojunction with the ample interfaces was prepared by the electrodeposition. A subsequent hydrothermal reaction modifies the 3D photoanode with surface Co_3O_4. The structural information of the p-n junction and chemical composition of the ternary compounds were characterized. And the Co_3O_4 decorated $CaFe_2O_4/\alpha\text{-}Fe_2O_3$ displayed an increased five times of photocurrent density (1.23 V vs RHE) and a cathodic shift of onset potential to 0.6 V vs RHE. The intrinsic mechanism was discussed on the basis of the electrochemical impedance spectra (EIS) and the open circuit potentials (OCPs) measurements. The formed p-n junction enhances the carrier separation in the bulk through the built-in electric field. Meanwhile, the Co_3O_4 plays a bifunctional role, namely, passivating the surface states and accelerating the water oxidation kinetics.

2. Experimental

Firstly, the Ca-containing FeOOH thin films were electrodeposited from a solution of 3.0 M NH_4Cl and 0.02 M $FeCl_2$. The atomic ratio of Ca and Fe in the film was tuned by adding a different volume of 0.1 M $Ca(NO_3)_2$ into the electrolyte of which the pH was adjusted to 7.0 by 1 M NaOH. The fluorine-doped tin oxide (FTO) glasses were ultrasonically cleaned in acetone, ethanol, and distilled water for 30 min, sequentially. The electrodeposition was performed in a conventional three-electrode cell using Bipotentiostat (Model AFCBP1) with FTO glass (1.5 cm × 2.5 cm) as working electrode. A platinum plate was used as counter electrode and an Ag/AgCl/sat. KCl electrode as reference electrode. The potential for electrodeposition was set to −0.2 V vs Ag/AgCl and the duration was in the range of 1–10 min. The films were annealed via a two-step treatment under 600 °C for 2 h and 800 °C for 15 min. Then the films were hydrothermally treated in an autoclave containing a mixture of 6.2 mg $Co(CH_3COO)_2{\cdot}4H_2O$, 375 µL ammonium hydroxide (25 wt%), and 25 ml ethanol at 393 K for 1 h. After naturally cooled to room temperature, the films were thoroughly washed with distilled water and dried in air.

The phase of the films was analyzed by XRD on a PANnalytical X'Pert diffractometer with a Co K_α radiation (λ = 0.178897 nm). The morphology and chemical information of the prepared films were investigated using SEM (JEM-7001F) and TEM (JEM-2100F) equipped with energy dispersive X-ray spectroscope (EDXS). The absorption characteristic of the film was conducted on a Lambda 750S UV–Vis Spectrometer with an integrating sphere using a bare FTO substrate as a reference. XPS was performed on Shimadzu Amicus using monochromatized Al K_α X-Rays (excitation energy 1486.8 eV). All binding energy (BE) values were determined with reference to the C1s line at 284.6 eV.

For clarity, the electrodes composing of pure $\alpha\text{-}Fe_2O_3$, binary ($CaFe_2O_4/\alpha\text{-}Fe_2O_3$), and ternary compound (Co_3O_4 loaded $CaFe_2O_4/\alpha\text{-}Fe_2O_3$) are denoted as $\alpha\text{-}Fe_2O_3$, Fe-Ca and Co-Fe-Ca, respectively, in the following context. The elemental compositions of the films are recorded by the atomic weight (at.%) of Ca and Co. For instance, when the Co, Ca and Fe is 2at.%, 1at.% and 97at.%, respectively, the sample is named 1at.% Co-Fe-2 at.% Ca.

The PEC performance of the prepared hematite photoelectrodes was carried out in a three-electrode electrochemical cell with Hg/HgO as the reference electrode, and platinum mesh (2 cm × 2 cm) as the counter electrode. The prepared films with an active area of 0.25 cm^2 were the working electrodes. The electrolyte was 1.0 M NaOH (pH = 13.6), which was deaerated with a nitrogen flow for 0.5 h before measurement. The linear sweep voltammetry (LSV) and chronoamperometry (I-t) measurements were performed. EIS data were gathered using 10 mV amplitude perturbation between 10,000 and 0.1 Hz. The light source was provided by a 300 W xenon lamp (CEL-HXF300) through AM 1.5 filter with a light intensity of 100 mW/cm^2. The light was irradiated from the substrate side.

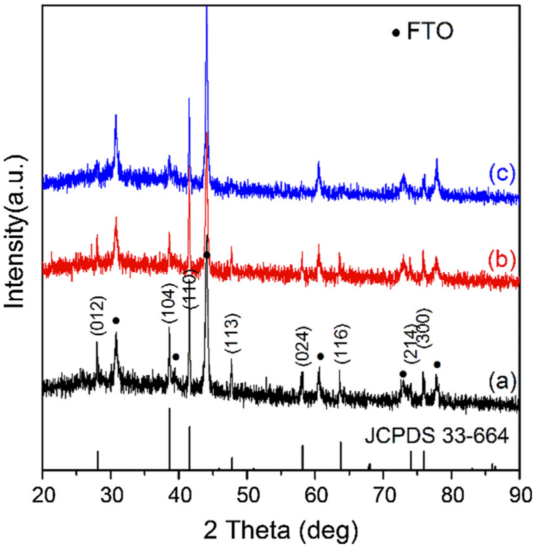

Fig. 1. XRD patterns of (a) $\alpha\text{-}Fe_2O_3$, (b) 1at.%Ca-Fe, and (c) 2at.%Co-Fe-1at.%Ca with the standard $\alpha\text{-}Fe_2O_3$ as reference. The films were electrodeposited at −0.2 V vs Ag/AgCl for 5 min.

The measured potentials with respect to Hg/HgO were converted against RHE using $E_{RHE} = E_{Hg/HgO} + E^0_{Hg/HgO} + 0.059pH$, where the $E^0_{Hg/HgO} = 0.098$ V.

3. Results and discussion

The crystalline structures of the as-synthesized $\alpha\text{-}Fe_2O_3$, binary, and ternary composite electrodes were analyzed using XRD. Fig. 1 shows the typical XRD spectra of three typical samples. The diffraction peaks at 28.1°, 38.7°, 47.8°, 58.1°, 63.7°, 74.0°, and 75.9° are assigned to $\alpha\text{-}Fe_2O_3$ (JCPDS No. 33-0664), and the rest of the peaks are due to the FTO substrate (JCPDS No. 46-1088). The thickness of the $\alpha\text{-}Fe_2O_3$ film could be controlled by the electrodeposition duration (Fig. S1). No diffraction peaks related to Ca- or Co-containing compounds are observed in Fig. 1. This could be due to the detection limit of XRD. It is worth noting that the addition of Ca^{2+} in the electrolyte promotes the preferential growth of hematite along the (1 1 0) plane, giving rise to the charge transport by considering the charge mobility anisotropy of hematite [28,29].

The chemical information of the $\alpha\text{-}Fe_2O_3$ and Co-Fe-Ca films was investigated by XPS, as shown in Fig. 2. The presence of carbon and nitrogen signals in the survey spectra is believed due to sample preparation and subsequent handling. The fine XPS spectra of Fe 2p in Fig. 2(b) show Fe $2p_{3/2}$ and Fe $2p_{1/2}$ peaks at 711.0 eV and 725.0 eV, respectively, as well as a satellite peak at around 719.2 eV. These are in consistent with the Fe^{3+} ions in the $\alpha\text{-}Fe_2O_3$ and $CaFe_2O_4$[16,19,42]. Because the XPS signals are surface sensitive, the Fe 2p peak intensities of the cobalt oxide covered composite film are weaker than that of the pure hematite. In Fig. 2(c), the Ca $2p_{3/2}$ and Ca $2p_{1/2}$ peaks are obtained at 346.8 eV and 350.5 eV, respectively [24,43]. In Fig. 2(d), the fine spectrum of Co 2p splits into Co $2p_{3/2}$ and Co $2p_{1/2}$ with binding energy (BE) at 780 eV and 795.5 eV, which fit well with Co_3O_4 in the literature [42]. In addition, the O1s peaks for the ternary composite film were fitted, as shown in Fig. 2(e). The fitting band at 530 eV is attributed to the lattice oxygen in the oxides ($\alpha\text{-}Fe_2O_3$, $CaFe_2O_4$, or Co_3O_4), accounting for about 75% of the total oxygen signal. The other fitting band at 531.9 eV belongs to the −OH group or the absorbed oxygen [5,42]. We thus concluded that the ternary compound consists of Co_3O_4, Fe_2O_3, $CaFe_2O_4$(Co-Fe-Ca), and the atomic compositions are shown in Table S2.

Fig. 3 shows the SEM morphologies of the prepared hematite films